PVP2014-28524

A METHOD TO IDENTIFY THE CRACK CLOSURE AND OPENING IN CYCLIC TEARING TESTS ON FRACTURE MECHANICS SPECIMENS

B. Tranchand
Tour AREVA, 92084 Paris La Défense, France
b.tranchand@gmail.com

V. Aubin
Ecole Centrale Paris
Chatenay-Malabry, France
veronique.aubin@ecp.fr

S. Marie
CEA DEN/DM2S/SEMT/LISN
CEA Saclay 91191Gif-sur-Yvette, France
stephane.marie@areva.com

ABSTRACT

To measure crack propagation in compact tension specimen, many methods can be used. The electric drop potential measurement is one of them and allows the detection of crack initiation. In our case, CT specimens, which have been taken from a carbon steel pipe (Tu42C) used in the secondary circuit of French PWR, are employed for cyclic tearing test. The detection of crack closure and crack opening should provide information for energetic analysis. However, the electric signal is unusable due to the cyclic loading. Indeed, because of the clearance between the pin and the specimen, each direction loading change causes a discontinuity in the signal. The roughness of the lips surface or the crack closure during compression loading returns also an unusual signal. Moreover, local measurement is required and there is high strain level around the crack tips, so strain gages are not suitable. Thus, displacement field are measured with digital image correlation and a specific image acquisition is employed. These methods allow a direct measurement of strain fields on the surface of the specimen. Thereby an interpretation of the previous electric signal and the crack opening and closure detection is realizable. Then, F.E. simulation, with non-linear kinematic hardening and node release method, are performed. These simulations allow the check of crack opening and closure detection through the specimen thickness.

INTRODUCTION

Currently, the analysis and the evaluation of the component integrity are realized by a cyclic J-integral in case of seismic loadings for nuclear application. This integral is calculated with the envelop curve of Load vs CMOD[1–3]. This approach, although conservative, doesn't care about the energy dissipated by the fracture for each cycle and has to be précised.

The calculation of the energy dissipated by the fracture for each cycle is our objective in this work. This is the reason why the identification of the different condition of the crack tip is essential in our work. In a first time, we tried the use of classical measurements: the electrical drop potential and strain gauge slicked behind the specimen. Unfortunately, these methods presented many disadvantage. Due to the high strain, the strain gauge became unstuck after few cycles. Moreover, the delivery signal for the first cycles was unusual. About the electrical drop potential measurement, it provided interpretable information at the minimum and the maximum of each cycle. That permitted to calculate the crack propagation at the maximum and to assume of the complete crack closure for the minimum. But between each other, it was difficult to make some assumption: due to the change of the pin support in the CT clevis hole, the electric configuration of the system changed. Then, a drop occurred. This fast description shows the importance to find another way to know the crack condition.

Hereafter, we will show that the digital image correlation technique could be a way for finding the crack condition for each point of a cycle.

Crack closure and crack opening identification will provide assumption for the electric drop measurement interpretation. Then, that could be support new assumption for the cyclic-J calculation.

NOMENCLATURE

a, W	= crack length and CT specimen width
ΔK	= variation of elastic stress intensity factor
$CMOD$	= Crack Mouth Opening Displacement
Δa	= crack extension
R	= load ratio (P_{min}/P_{max})
$I.D. / O.D.$	= Inner / Outer Diameter

EXPERIMENTAL DESCRIPTION

The pipe (219.1 mm O.D. and 186.9 mm I.D.) used in this study is a made of Tu42C, a ferritic steel used in secondary heat transport in French nuclear power plant. Chemical compositions and tensile properties are given below (Table 1 and Table 2) [4]. CT specimens of thickness 12 mm and other dimensions conforming to ASTM Standard E1820 [5] were machined from the pipe. These specimens were used to characterize the fracture resistance of the considered materials.

1

Copyright © 2014 by ASME

The specimens were machined in the L-C orientation with respect to the pipe axis: thus the notch was representative of a circumferential defect in a pipe.

Table 1 Chemical composition in wt %

Material	C	Si	Mn	P	S	Cu	Sn
Tu42C	0.19	0.19	0.77	0.013	0.006	0.02	0.003

Table 2 Tensile properties

E (MPa)	σ_y (MPa)	σ_u (MPa)	El (%)
204 000	310	470	35

Prior to each test, a fatigue pre-cracking had been performed on a 50kN servo-hydraulic tensile test machine. The fatigue pre-cracking had been performed with decreasing loading level with a ΔK value going from 25 MPa to 12 MPa and a R=0.1 load ratio. The crack length-to-width ratio had been defined for all specimens to the value of 0.5.

The cyclic tests were carried out on the same servo-hydraulic machine. The following quantities were monitored and recorded:

- the CMOD using a MTS clip gage ;
- the applied load using the load cell in the actuator.

Figure 1 shows the cyclic toughness test system.

On the right of the tensile test machine (Figure 1), there is an image acquisition system. A W&B camera with a resolution of 8 Mpx is linked with another data acquisition computer. That permits to link picture and test quantities, as elapsed time, load and CMOD.

A particular attention is required to the image data acquisition made with Labview software. Indeed, our program construction allowed us to register images every increment of time (a constant rate of time), CMOD or load. As a too low increment could cause a saturation of the CPU, the increment chosen is a compromise between the CPU occupation and the precision between two picture captions.

We chose to save our picture under constant rate of CMOD.

Moreover, the lighting took an important part in the quality picture. Many lights have been tested like LED, incandescent, halogen and optic fiber lights. The more efficient was a halogen light. However, the exposure time of the camera had to be adjusted to be higher than the light frequency. Otherwise, bands appeared on the picture.

As there are no testing standards currently, the testing procedure is implemented in the software MTS TestSuite™. The diagram of the loading sequence is presented in Figure 2 below. In red color, the test is under displacement control, in blue color, under load control.
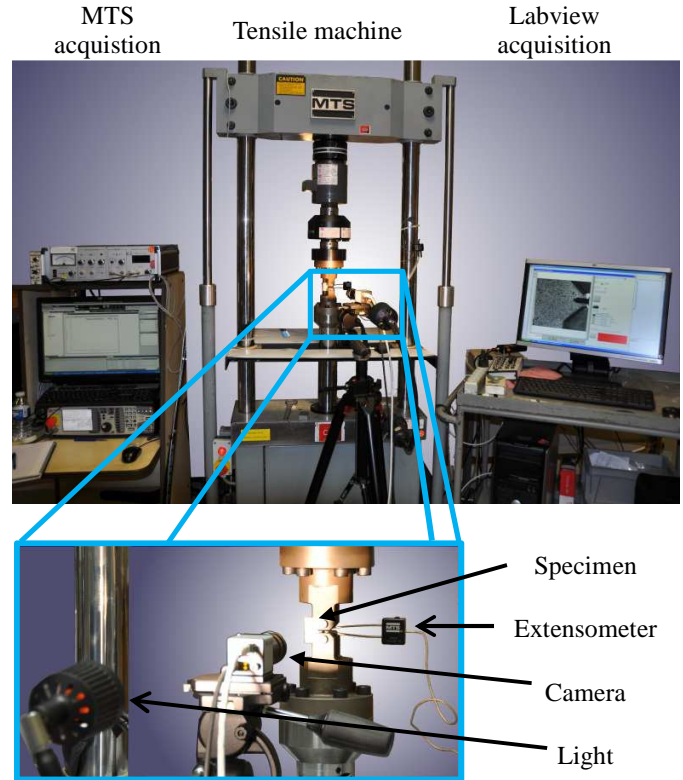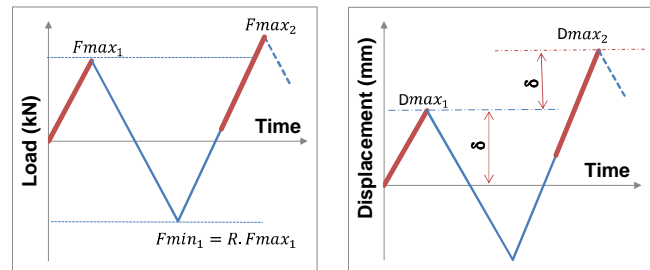

Figure 1 Testing device

Figure 2 Loading diagram

During the first step, a displacement increment δ was imposed. After the storage of the maximum load F_{max_1} and the maximum displacement D_{max_1}, the load decreased down to the minimum load calculated with $F_{min_1} = R.F_{max_1}$. Then, the load increased up to $2kN$. Thereafter, the displacement increased to $D_{max_2} = D_{max_1} + \delta$ and the new maximum load F_{max_2} was saved.

The loading details are as follows:

- the load ratio was $R = -1$;
- A constant displacement increment δ was applied after every cycle. For these tests, an increment of 0.2 mm was chosen.

Copyright © 2014 by ASME

The displacement and the load speeds are as follow:
- 0.02 mm/s;
- 0.2 kN/s.

These speeds are lower than classic test in order to obtain a better quality of our pictures.

The Table 3 summarizes tests presented in this study.

Table 3 Tests matrix

Specimen	R	δ	B	Bn	a0	af	Δa
		mm	mm	mm	mm	mm	mm
736A-H	◆		12	9.6	12.00	15.30	3.30
736A-Q	■	-1	0.2	12	9.6	12.42	16.27	3.85
736A-AL	▲			10.8	10.8	-	-	-

It should be noticed that the side grooves had been removed for the digital image correlation. Indeed, the sides grooves would not allowed a correct displacement field measurement. This modification on the CT geometry led to some particularity on the crack behavior due to the plane stress. These particularities will be presented in the following paragraph.

Two other correlation tests had been performed with an $R = -1$ imposed load ratio: one with $\delta = 0.2mm$ and the other with $\delta = 0.3mm$. The first had not a satisfying image quality and the second was not reproducing with a "classic" cyclic test.

Principle of digital image correlation

The software used for the image correlation is CorreliQ4 [6]. This software was developed in the French university of LMT-Cachan by F. Hild and S. Roux.

Briefly speaking, the principle of this software is the comparison of two digital images: a reference image and an image of the same zone obtained after a mechanical loading. A mesh is built on the reference image. A correlation method is used to match each element of the reference image to the corresponding one in the deformed image. This allows to obtain a displacement field which is then derivate to obtain the strain field. The principle of digital image correlation is described in references [7,8].

Tests results

Comparison with cyclic tests

Hereafter, Figure 3 compares a "classical" cyclic test Load-CMOD curve with a "correlation" cyclic test. The difference between the two curves is consistent: the lowest maximum load is explained by the dimension of the correlation specimen, which had no more side grooves.

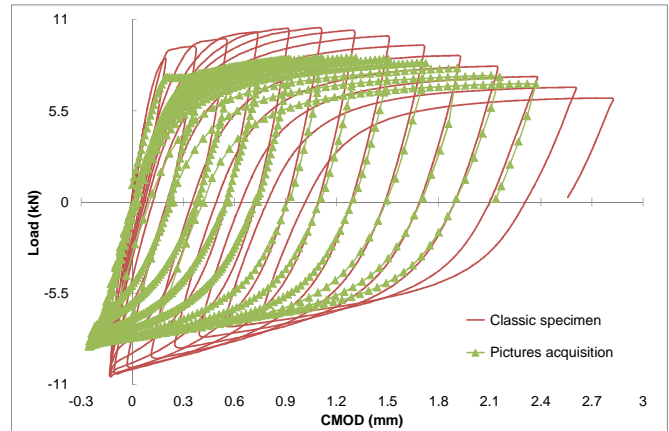Each green point on the figure represents one image.

Figure 3 Comparison of Load-CMOD curves between a classic test and a correlation test

Surface fractures obtained with a correlation specimen or classical specimen are then compared.

The fatigue pre-crack is straighter for the correlation specimen (Figure 4(b)). The crack propagation is less important. Indeed, there was less cycle during the correlation test. It was interrupted earlier because of the bifurcation on the side of the specimen (Figure 5). This bifurcation is a result of the plane stress.

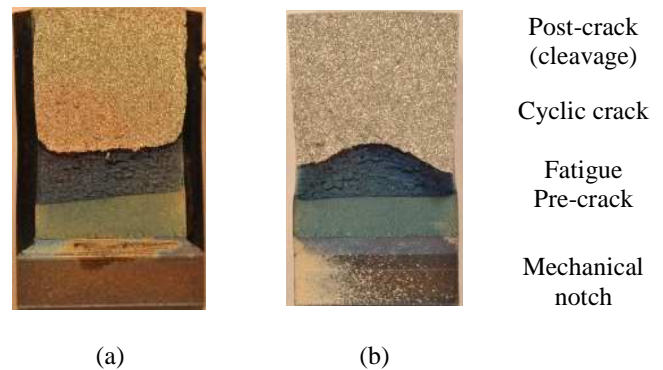Furthermore, the front of the crack is not straight always due to the lack of the side grooves.

Post-crack (cleavage)

Cyclic crack

Fatigue Pre-crack

Mechanical notch

(a)   (b)

Figure 4 Comparison of the surface fractures between a classical specimen (a) and a correlation specimen
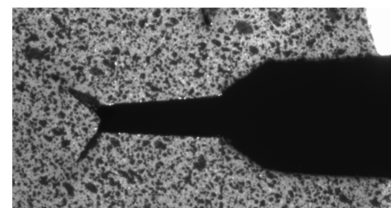

Figure 5 Illustration of the crack tip's bifurcation at the end of the test

Because of the plane stress, the interpretation of the displacement field and particularly of the strain fields will be cautious.

Quality of the images

Figure 6 shows an image obtained at the beginning of the test. The region of interest chosen for the next analysis is illustrated by the yellow dot rectangle. The spatial resolution of the picture is as following:
- 1 pixel = 7.9 µm;
- 1 mm = 127 pixels.

As mentioned before, the light is important for the picture quality. The grey histogram has to be as large as possible. Figure 7 shows the result of the light optimization and camera settings.
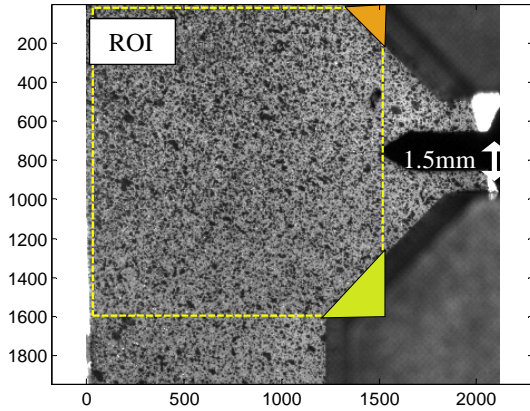

Figure 6 First picture of the test (F=0kN) with the chosen Region Of Interest.
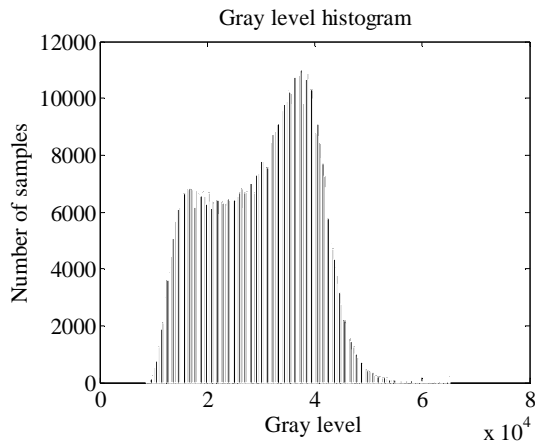
Figure 7 Grey level histogram in the ROI.

The next figures (Figure 8 and Figure 9) qualify the image correlation performances. They provide information for the choice of the size mesh used by Correli_Q4. It should be noticed that the choice of the mesh size is a compromise between a fine mesh which leads to a very fine spatial resolution, and then the measurement of local gradients, and a rougher mesh which improves the precision and minimizes errors.

A prescribed displacement is imposed by translation of the original picture by a given displacement. The displacement field is calculated between these two images using Correli_Q4.

If the calculation would be perfect, the displacement field calculated should be uniform and equal to the prescribed one. The difference between this theoretical value and the average of the calculated displacement is called mean error and is plotted in Figure 9 with respect to the mesh size. The standard uncertainty is plotted in Figure 8. It can be seen that the mean error and the standard uncertainty increase when the mesh size decreases. In order to guarantee a precision sufficient, a mesh size of 16 pixels (or 0.126 mm) was chosen in this study (Figure 10). The mean error is then of 0.002 pix and the standard uncertainty of 0.5.
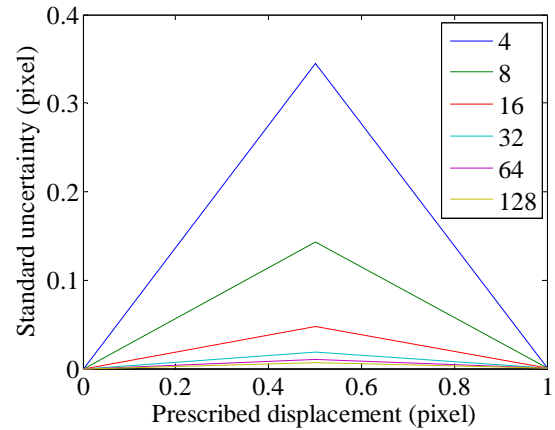

Figure 8 Analysis of the mean error obtained by DIC between 2 images as a function of the prescribed displacement for several mesh size.
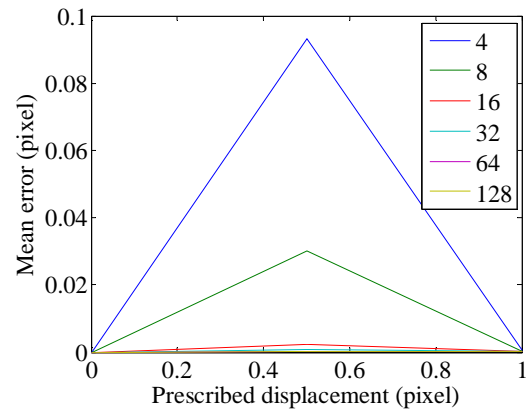

Figure 9 Analysis of the standard uncertainty by DIC between 2 images as a function of the prescribed displacement for several mesh sizes.
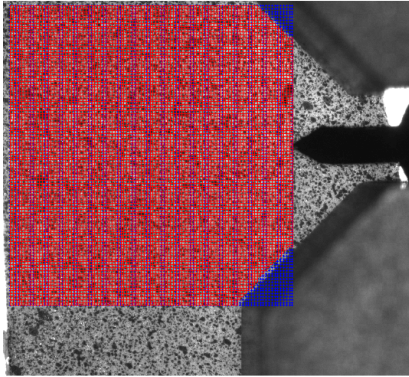
4   Copyright © 2014 by ASME

Figure 10 Illustration of the chosen mesh.

Crack closure detection

The principle of the crack closure determination is based on the continuity of the vertical displacement field.

The presence of a crack creates a discontinuity of the displacement field, as the points on both sides of the crack move in the opposite directions, which is illustrated in Figure 11.

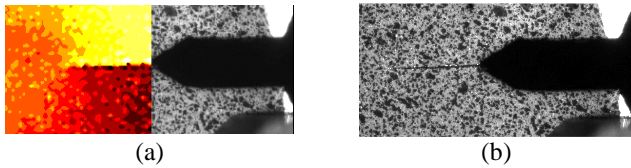(a)   (b)

Figure 11 Principle of the crack closure detection assumption: (a) image of the crack, (b) vertical field displacement, in red the displacement is negative and in yellow positive. The loading is vertical starting at the bottom.

On the other hand, the displacement field of a closed crack would be continuous from one side to the other one, as illustrated in Figure 14(d).

Figure 14(a) to (d) were obtained using CorreliQ4 by the comparison of two successive images taken during the compressive part of a cycle (Figure 12).

During the load decreasing, when the crack is not closed, the vertical displacement field shows a discontinuity, as the upper and lower parts of the specimens get closer. Displacement fields shown in Figure 14 (a) to (d) were obtained with a same increment of the CMOD: 0.01 mm. It is possible to observe in Figure 14 that the intensity of the displacement field is the same in steps (a) and (b) and decreases in step (c).

Finally, in Figure 14 (d), there is no more discontinuity; the level of the field displacement is very small despite the constant $\Delta CMOD$ between the images used for the correlation. The entire crack is now closed.
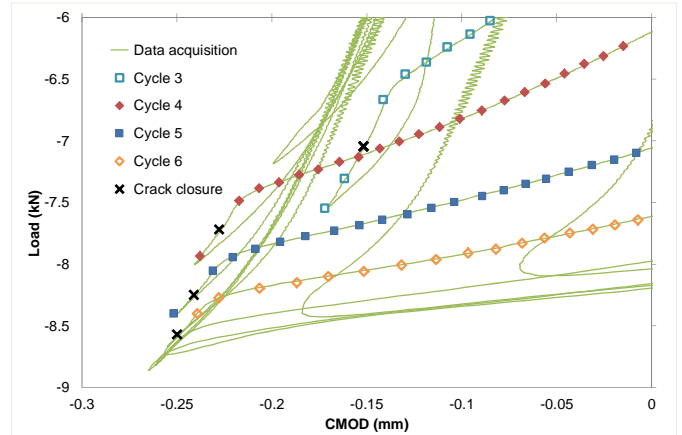

Figure 12 Illustration of the crack closure condition in the Load-CMOD for few cycles.

Crack closures detected with the method presented above have been compared to DDP-CMOD curves obtained from "classical" tests. Time of crack closure coincide with the suddenly decreased of DDP versus CMOD. This allows to use directly the DDP-CMOD curve (Figure 13) as an indication of crack closure.
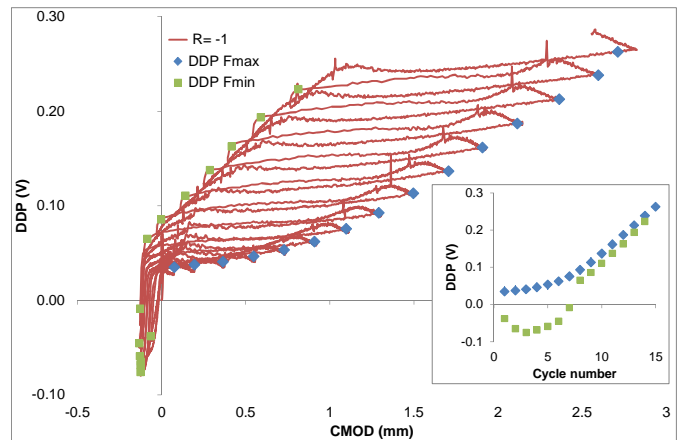

Figure 13 DDP-CMOD curve for a classical R= -1 test.

5   Copyright © 2014 by ASME

-7.34 kN
< Load <
-7.38 kN

-0.20 mm
< CMOD <
-0.21 mm

(a)

-7.38 kN
< Load <
-7.48 kN

-0.21 mm
< CMOD <
-0.22 mm

(b)

-7.48 kN
< Load <
-7.71 kN

-0.22 mm
< CMOD <
-0.23 mm

(c)

-7.71 kN
< Load <
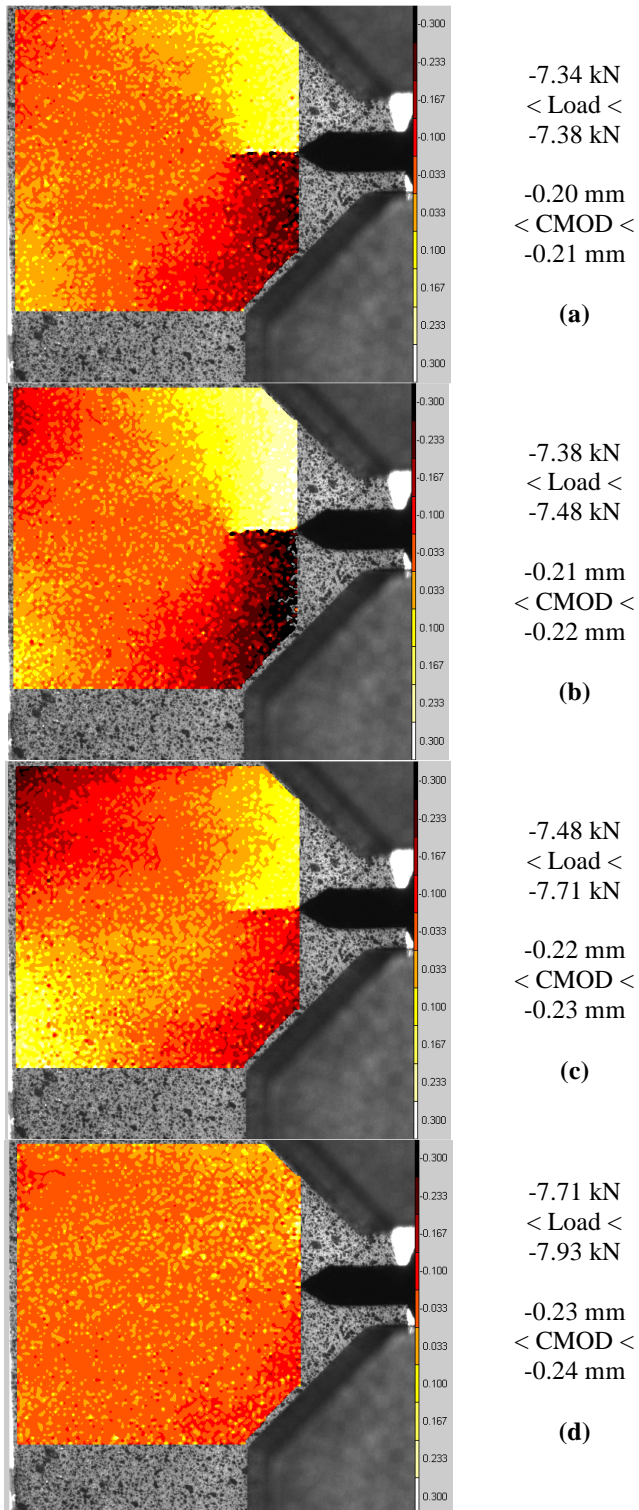-7.93 kN

-0.23 mm
< CMOD <
-0.24 mm

(d)

Figure 14 Vertical displacement field: illustration of the crack closure interpretation obtained for four consecutive image correlations at the 4th cycle.

-7.28 kN
< Load <
-7.11 kN

-0.15 mm
< CMOD <
-0.14 mm

(a)

-7.11 kN
< Load <
-6.84 kN

-0.14 mm
< CMOD <
-0.13 mm

(b)

-6.84 kN
< Load <
-6.44 kN

-0.13 mm
< CMOD <
-0.12 mm

(c)

-6.44 kN
< Load <
-5.47 kN

-0.12 mm
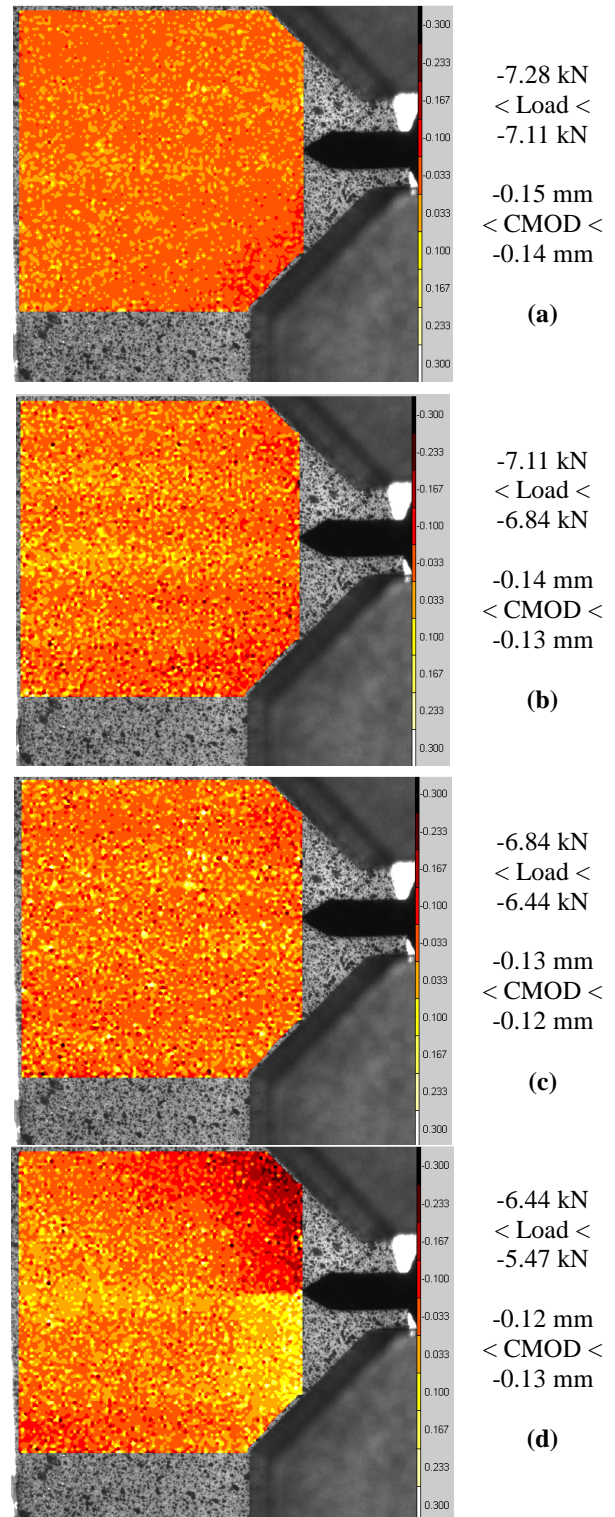< CMOD <
-0.13 mm

(d)

Figure 15 Vertical displacement field: illustration of the crack opening interpretation obtained for four consecutive image correlations at the 3rd cycle.

6

Copyright © 2014 by ASME

Crack opening detection

The same method was used to detect crack opening, as illustrated in Figure 15 and Figure 16.
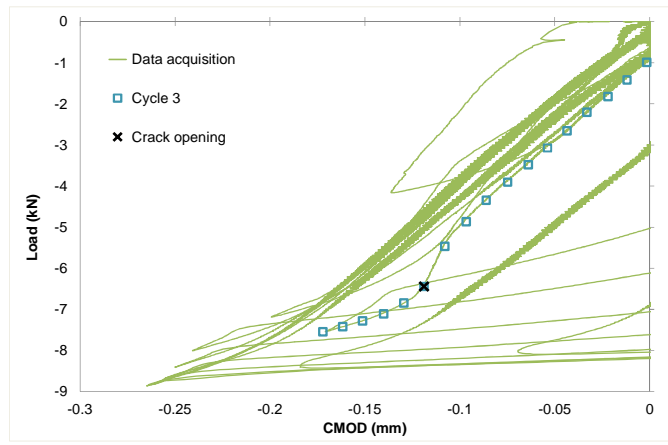

Figure 16 Illustration of the crack opening condition in the Load-CMOD for the 3rd cycle

Prospects

Crack propagation

Calculations for correlation of the digital images taken at a positive load are under progress.

With a similar method, we will try to detect the crack propagation.

FE analysis

F.E analysis was realized with the F.E. CASTEM. CT cyclic tests have been simulated with a non-linear hardening law. The simulation was built the same way as the experimental one: in load and displacement control. The crack propagation was performed with node release, controlled with the results of the tests.

Hereafter, in Figure 17, there are the first results of these simulations compared with the third cycle of the previous test. Below this curve, there are the illustrations of the contact between the crack surfaces for the three first cycles. First of all, the blue area is on contact, symbolized by the blue point on the curve. Then, the pre-crack surface begins to be on contact with each other which is represented by the red area and the red point on the curve.

These simulations would provide the crack closure conditions in the middle of the CT specimen as image correlation permits its determination on the surface of the crack specimen.
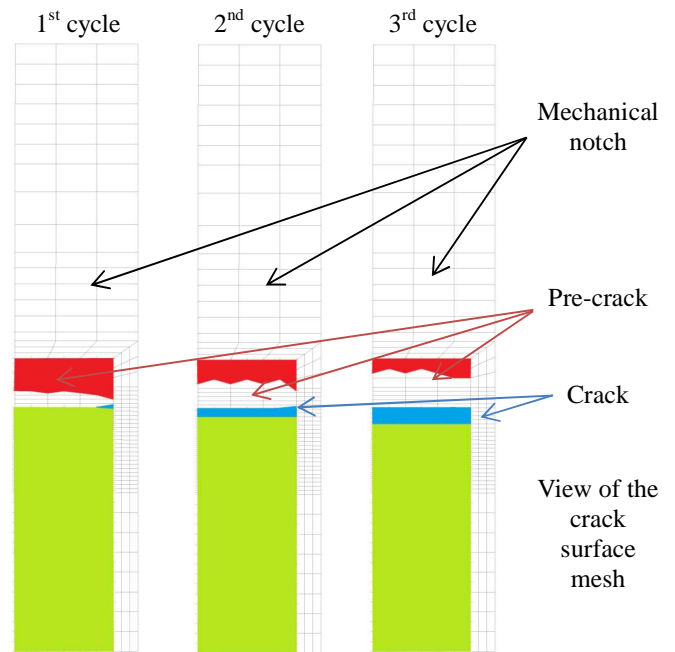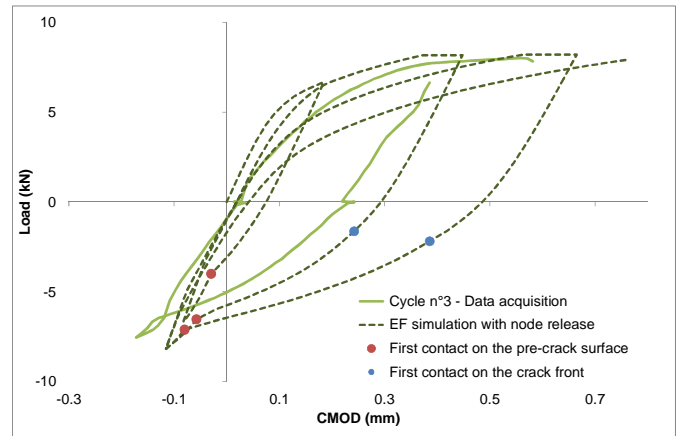

Figure 17 First E.F. simulations of cyclic tests and crack closure analysis for the three first cycles.

REFERENCES

[1] Rudland DL, Brust F, Wilkowski GM. The Effects of Cyclic and Dynamic Loading on the Fracture Resistance of Nuclear Piping Steels. Technical Report, October 1992--April 1996. Nuclear Regulatory Commission, Washington, DC (United States). Div. of Engineering Technology; Battelle, Columbus, OH (United States); 1996.

Copyright © 2014 by ASME

[2] Seok C-S, Murty KL. A study on the decrease of fracture resistance curve under reversed cyclic loading. Int J Press Vessels Pip 2000;77:303–11.

[3] Singh PK, Ranganath VR, Tarafder S, Prasad P, Bhasin V, Vaze KK, et al. Effect of cyclic loading on elastic–plastic fracture resistance of PHT system piping material of PHWR. Int J Press Vessels Pip 2003;80:745–52.

[4] Le Corre V. Étude de la compétition déchirure ductile/rupture fragile: Application à la tenue mécanique des tubes en acier C-Mn et de leurs joints soudés. Ecole Centrale de Lille, 2007.

[5] E08 Committee. Test Method for Measurement of Fracture Toughness. ASTM International; 2009.

[6] Hild F, Roux S. Correli Q4: A software for-finite-element-displacement field measurements by digital image correlation. Rapp Interne LMT Cachan 2008;269.

[7] El Bartali A, Aubin V, Degallaix S. Fatigue damage analysis in a duplex stainless steel by digital image correlation technique. Fatigue Fract Eng Mater Struct 2008;31:137–51.

[8] Roux S, Hild F. Stress intensity factor measurements from digital image correlation: post-processing and integrated approaches. Int J Fract 2006;140:141–57.

Copyright © 2014 by ASME